Available online at www.sciencedirect.com
SCIENCE DIRECT®
Mechanics of Materials 35 (2003) 129–154
MECHANICS OF MATERIALS
www.elsevier.com/locate/mechmat

Cleavage crack-growth-resistance of grain boundaries in polycrystalline Fe–2%Si alloy: experiments and modeling

Y. Qiao, A.S. Argon *

Department of Mechanical Engineering, Massachusetts Institute of Technology, Cambridge, MA 02139, USA

Received 18 June 2002

Abstract

Experiments were carried out on the modes of advance of cleavage cracking through a field of randomly oriented grains at −30 °C in the pure cleavage range (lower shelf) in very large grain size Fe–2%Si alloy, permitting detailed observations of the chronology of percolation of the cleavage crack front across a field of grains. Utilizing previously developed model-based information on the peak resistance to fracture of high angle grain boundaries, with a given tilt and twist misorientation across them, and detailed measurements of orientations of individual grains in the samples, it was possible to develop percolation maps of cleavage through the field of grains that for the initial phases of fracture through grains predicted the actual path with about 70% accuracy when compared with experimental observations. On the basis of these experiments and modeling a simple expression is projected for the effect of grain boundaries on the overall cleavage fracture resistance of low-carbon steel in the lower shelf region. The model gives a nearly 3-fold rise of cleavage resistance of the polycrystal over the single crystal, substantially independent of grain size. Additional experiments on decarburized 1010 steel of 50 μm grain size with an unusually low brittle-to-ductile transition temperature gave very similar results on the mode of percolation of cleavage cracking through grains even though in this case the cleavage propagation was under upper shelf conditions.

Keywords: Cleavage in polycrystals; Percolation of cleavage through grains; Cleavage resistance in the lower shelf

1. Introduction

High angle grain boundaries in steel offer an important resistance to the propagation of cleavage cracks, particularly in the brittle-to-ductile transition region. While there has been much emphasis on grain size effects on the plastic resistance (Hall, 1951; Petch, 1953) and the beneficial effects of grain size reduction on raising the brittle strength are well known (Petch, 1954), the specific role of grain boundaries in affecting cleavage crack growth resistance has not been clarified. Based on observations in hydrogen charged Fe–3%Si (by weight) alloy, Gell and Smith (1967) noted that the resistance of grain boundaries to the transmission of cleavage cracks across them is governed more importantly by the twist misorientation than the tilt misorientation across the boundary. They attributed this to a difficulty in initiating new

* Corresponding author. Tel.: +1-617-253-2217; fax: +1-617-258-8742.
E-mail address: argon@mit.edu (A.S. Argon).

0167-6636/03/$ - see front matter
PII: S0167-6636(02)00194-1

cleavage cracks in the neighboring grains that would indeed be more strongly influenced by the twist misorientation. Crocker et al. (1996) studied specific forms of break-through across boundaries and classified them into four types related to the observed features of fracture along boundaries. In a quite detailed modeling study Anderson et al. (1994) considered the mode of propagation of cleavage cracks across hexagonal grains and demonstrated that the cumulative probability of overall fracture in a "weakest link" context of triggering brittle response in structures is directly influenced by the impediments that grain boundaries have on cleavage crack propagation. To our knowledge the only detailed model of the role of grain boundaries on impeding the percolation of cleavage cracks across a field of randomly misoriented grains in steel is that of McClintock (1997). In this he stated a number of criteria of overcoming individual grain boundaries by a quasi-statically advancing cleavage front and estimated the specific work of fracture due to plastic shear on grain boundaries bridging primary cleavage facets of adjoining cracked grains. There have been no corresponding experimental studies of these phenomena.

In a recent study of the modes of cleavage crack transmission across specific bicrystal grain boundaries in a special Fe–3%Si alloy Argon and Qiao (2002) and Qiao and Argon (2003a) have measured the specific break-through resistances of 17 different high-angle boundaries with random combinations of tilt and twist misorientations and associated these measurements with measurements of fractographic features of these break-through processes. The resulting geometrically based boundary resistance model provided an excellent fit to the measured break-through resistances, taking the 17 boundaries as a whole.

In the present study we have extended the above bicrystal experiments to the growth of cleavage cracks through a field of very coarse grains in a Fe–2%Si alloy and followed the percolation of the cleavage process from grain to grain in considerable detail. These findings have then been incorporated into a model that quite successfully paralleled the experimental observations. On the basis of these findings we have stated a simple relationship for the overall contribution of grain boundaries to cleavage crack-growth-resistance in the lower shelf region. The experiments and the model are in agreement with many, but not all, of the predictions of McClintock's (1997) model referred to above.

Finally, to probe the application of our findings to low carbon steels we have carried out experiments on medium grain size (~50 μm) decarburized 1010 commercial steel. While this material, in view of its unusually low plastic resistance, had a very low brittle-to-ductile transition temperature, most of the geometrical features of percolation of cleavage fracture through grains were very similar to the observations in the Fe–2%Si coarse grained material, even though in this case such cleavage percolation was representative of conditions at the upper shelf, on the basis of specific fracture work.

2. Experimental details

2.1. Materials

For the present investigation of the forms of brittle crack propagation across a field of grains in polycrystals, two complementary materials were selected. One was a very coarse-grained (in the range of 4 mm) Fe–2%Si alloy to complement the previous investigation of the fracture resistance of individual grain boundaries (Argon and Qiao, 2002; Qiao and Argon, 2003a). The other was a fine-grained decarburized 1010 steel of roughly 50 μm grain size. The Fe–2%Si alloy was provided in square pieces cut from hot rolled plates manufactured by Armco Metals of Middlefield, Ohio, with a thickness of approximately 26 mm, and lateral dimensions of about 30 by 30 cm. The material came from a batch used in an investigation on hot working of metals by Brown et al. (1989). [1] In the as-received material, there were small carbides of a size below 5 μm. To avoid undesirable interactions of such carbides with the cleavage crack propagation in the matrix, the material was annealed

[1] We are grateful to Professor Anand for making this material available to us.

and decarburized according to a stringent schedule (Birks, 1969; Thelning, 1984) that had been used also in the earlier studies of Argon and Qiao (2002) and Qiao and Argon (2003a). The decarburization schedule consisted of first breaking-down the carbides by a prolonged period of 60 h of soaking the alloy at 1400 °C in a pure nitrogen environment followed, without interruption, by a holding time of 2.5 h at 1200 °C in a hydrogen environment, and ending up with a slow furnace cool to prevent entrapment of and enbrittlement with hydrogen. After the decarburization, no carbides could be observed on fracture surfaces by SEM. The Vickers hardness of this material after the decarburization was 226 kg/mm^2. As already stated, the grain size of this alloy was quite coarse and in the range from 3 to 10 mm with a few grains being as large as 30–50 mm. Based on the visual examination of low temperature fracture surfaces of individual grains, which will be described in detail in Section 4.2, the orientation of grains appeared reasonably random. The chemical composition of the Fe–2%Si is given in Table 1.

To determine the relevance of the findings on the Fe–2%Si alloy to structural steels, a 1010 steel was chosen as the second material for study. The 1010 steel was provided in the form of rolled plates furnished by Oliver Steel Plate of Twinsburg, Ohio. The as-received material was in slabs of 26 mm thickness and with lateral dimensions of 30 by 60 cm, with an original carbon content of about 0.1%. To render this low carbon steel single phase, without a complicating pearlite component, it was subjected to a similar annealing and decarburization process described above for the Fe–2%Si alloy. After the decarburization, the carbon content was reduced to less than 0.05% with all of it being in solution. No carbides or a pearlite component could be detected. The grain size of the decarburized 1010 steel was in the range from 20 to 50 μm. Its Vickers hardness at room temperature was 179 kg/mm^2.

2.2. Specimen preparation

Compact fracture toughness tests (ASTM standard E399) were performed on the decarburized Fe–2%Si alloy. Standard fracture specimens were machined from the material, having dimensions of width $w = 63.5$ mm, thickness $b = 20.3$ mm, height $h = 1.2w = 76.2$ mm and initial crack length, a_0, in the range of about 39 mm. All samples were pre-fatigued to produce well characterized sharp initial pre-cracks.

The decarburized 1010 steel specimens were machined into double-edge cracked plate (DECP) shapes, of width $w = 19.1$ mm, thickness $b = 4.0$ mm, and initial crack length $a_0 = 2.5$ mm. The edge cracks were electrical discharge machined (EDM) in the mid-plane of the gauge area by using a 0.1 mm copper EDM wire. The machined specimens were annealed for 2 h at 600 °C.

2.3. Testing procedures

The fracture tests on the compact fracture toughness specimens of Fe–2%Si and DECP specimens of the decarburized 1010 steel were carried out on a Type 5508 Instron machine with a Type 319-007 environmental chamber. The specimens were tested at temperatures ranging from −30 °C to as high as 350 °C. For the high-temperature experiments, the environmental chamber was filled with dry nitrogen gas to prevent oxidization of the fracture surfaces. During the experiments, loads and load-point-displacements were measured and recorded continuously through the machine load cell and the LVDT of the Instron machine. For the compact fracture toughness tests of Fe–2%Si alloy, the temperature range covered the entire set of phenomena of pure-cleavage to a transition to mixed-cleavage behavior around 0 °C, to the conventional brittle-to-ductile transition temperature at around 250 °C and beyond up to 350 °C.

Table 1
Composition in weight fractions of the Fe–2%Si alloy

Element	C	Si	Al	Mn	Cu	Cr	Ni	Mo
Content (%)	<0.1	1.98	0.56	0.16	0.26	0.13	0.14	0.038

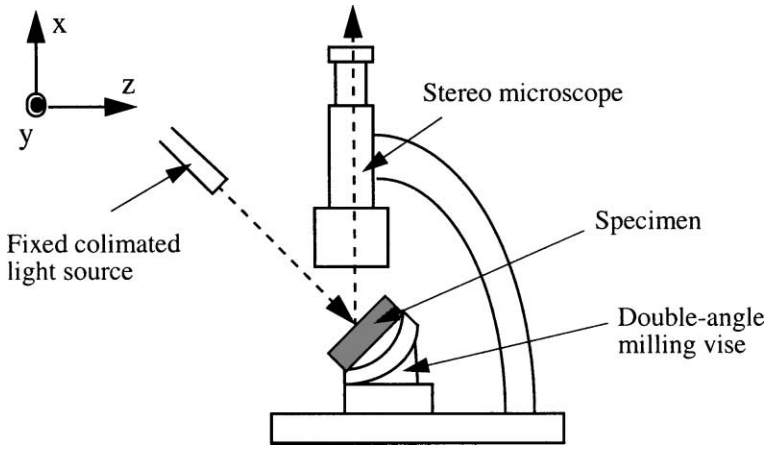

Fig. 1. Sketch of the modified stereo microscope for determination of inclination of cleavage planes in individual grains relative to sample reference surfaces.

For the fracture tests on the DECP specimens of decarburized 1010 steel, to reach the lowest possible temperature, a cryogenically rated solenoid valve controlled by an Omega JK12 controller was installed in the piping system of liquid nitrogen to control the low temperature nitrogen gas flow into the chamber responding to the feedback signals from the thermocouple directly attached to the specimen surface. For these lowest temperature tests the commercial temperature controlling system of the chamber was deactivated. Temperature uniformity in the DECP specimens was reached typically within 15 min. However, as already stated above, due to the very low carbon content in the decarburized 1010 steel and the absence of other hardening agents, even at the lower limit of −150 °C of this special environmental chamber the fracture behavior of the material remained to be above its brittle-to-ductile transition temperature.

2.4. Methods of fracture surface characterization

To study the forms of interaction between propagating cleavage cracks and grain boundaries, fracture surfaces across the field of fractured grains of three of the Fe–2%Si specimens were characterized in detail. For this purpose a special device was produced to measure the tilt and twist orientation of cleavage fracture surfaces of each individual grain with respect to the lateral specimen surface and the expected median geometrical plane of the desired crack propagation. The device is shown in Fig. 1. The stage of a stereo microscope was replaced by a double-angle vise having a base capable of rotating 360° about a vertical axis (x) and able to incline from horizontal by 45° up or down about an axis (y), with attached goniometers permitting the rotation angles to be measured to within ±0.5°. A parallel light source was fixed on the frame of the stereo microscope as shown in the figure. The system was first calibrated by means of a mirror placed in such a position as to reflect the light from the light source into the microscope tube along its optic axis. Then the mirror was replaced by the fractured specimen to be characterized. By rotating the vise along the x- and y-axes, the position of the specimen was adjusted so that cleavage facets of each individual grain reflected the light into the microscope. In this way the tilt and twist angles for each grain in the fracture field relative to the external specimen axes could be measured and recorded. The relative tilt and twist angles between individual grains across their common grain boundaries could then be readily calculated from this information, as discussed in Section 4.3.

Through viewing the cleavage surfaces of each grain of the fractured coarse-grained Fe–2%Si alloy, the break-through patterns and river mark-

ings could also be determined to establish in each case the grain boundary which was penetrated-through first by the propagating cleavage crack. The results were reported as fracture propagation maps to be presented in Section 4.2.

3. Experimental results

3.1. Temperature dependence of plastic resistances

Since the brittle-to-ductile transition behavior of metals and alloys, particularly the two iron based materials of Fe–2%Si and the decarburized 1010 steel, is governed primarily by the temperature dependence of their plastic resistance, this information was established first. Fig. 2 shows the results for these two materials. The information on the Fe–2%Si alloy was obtained by re-scaling the corresponding information of the Fe–3%Si alloy reported by Qiao and Argon (2003a). The re-scaling was accomplished on the basis of the ratio of the Vickers hardnesses of these two alloys at room temperature. The information on the decarburized 1010 steel was developed through direct determination of the stress-strain behavior of this material in tension experiments carried out at different temperatures, in the same environmental chamber discussed above.

Fig. 2 shows that the expected brittle-to-ductile transition temperature of the two materials will be quite different, based primarily on the temperature dependence of their plastic resistances, as we will amplify further in Section 5.3. The horizontal dotted line related to the curve for the Fe–2%Si alloy together with the large scatter at low temperatures results from the widespread twinning in the single crystals of the Fe–3%Si alloy tested in a multiple slip orientation that was reported in the previous study. From that study it is also known that the temperature dependent yield stress curve and the corresponding fracture stress curve come together at around 680 MPa and −60 °C, indicating that under these conditions yielding and fracture are simultaneous. From this we estimate the brittle strength of the Fe–3%Si alloy to be 680 MPa and assume that this magnitude should also be close to the brittle strength of the very coarse grained Fe–2%Si alloy of interest to us here. Noting that the average grain size of the Fe–2%Si

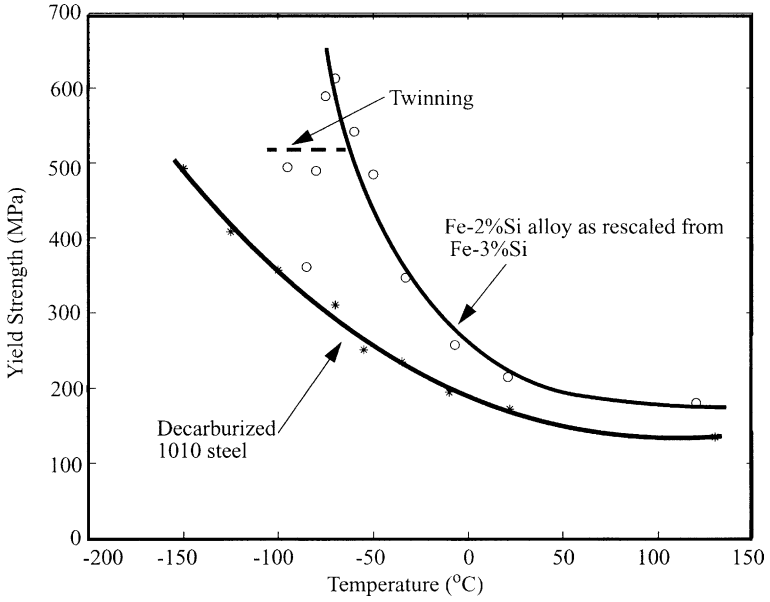

Fig. 2. Temperature dependence of tensile yield stresses in Fe–2%Si alloy (as scaled from data on Fe–3%Si single crystals) and decarburized 1010 steel.

alloy samples was around 4 mm and that of the 1010 steel was around 50 μm, and that the brittle strength should scale inversely with the square root of the grain size, we estimate the brittle strength of the decarburized 1010 steel to be well above 1.0 GPa.

Parenthetically, we note that after decarburization, to a 0.05 wt% C it is improper to refer to the decarburized 1010 steel as a *steel*. It should best be referred to as commercial purity iron. Nevertheless, because of its original designation we will continue to refer to it as decarburized 1010 steel.

3.2. Compact fracture experiments on the Fe–2%Si alloy

Fig. 3 shows the dependence on temperature of the measured K_{IC} fracture toughness of the Fe–2%Si alloy. The figure shows clearly two kinds of fracture work transition, one at around 0 °C and the other at around 250 °C. The first, and the one involving the small change in fracture work at 0 °C was identified to be the pure-cleavage to mixed-cleavage (PC/MC) transition reported by Qiao and Argon (2003a) in their experimental study of fracture resistance of individual bicrystals in Fe–3%Si alloy. In that study it was found that below the transition temperature when a cleavage crack breaks through a grain boundary into a neighboring grain, the break-through occurs at roughly evenly spaced "gates" and forms a tiered cleavage surface in the adjoining grain, resulting in a set of quasi-regularly spaced cleavage strips resembling a staircase, with the descent angle of the staircase being governed primarily by the twist misorientation of cleavage planes across the boundary. In the transit of the cleavage crack across the grain boundary in the pure cleavage (PC) range, below the transition temperature, the peak cracking resistance is governed by the rate of increase with respect to crack advance of: (a) primarily the additional cleavage surface production in the adjoining grain; and (b) secondarily, the increase in plastic shearing work at the grain boundary along the cleavage steps. Above the PC/MC transition, the geometrical features of the transit of the cleavage crack appear nearly identical to those below the fracture transition. However, additional plastic work is involved in sigmoidal plastic bending of ligaments between the cleavage strips in the adjoining grain before the ligaments are eventually severed by cleavage or by a cleavage-like separation, with the additional plastic bending of

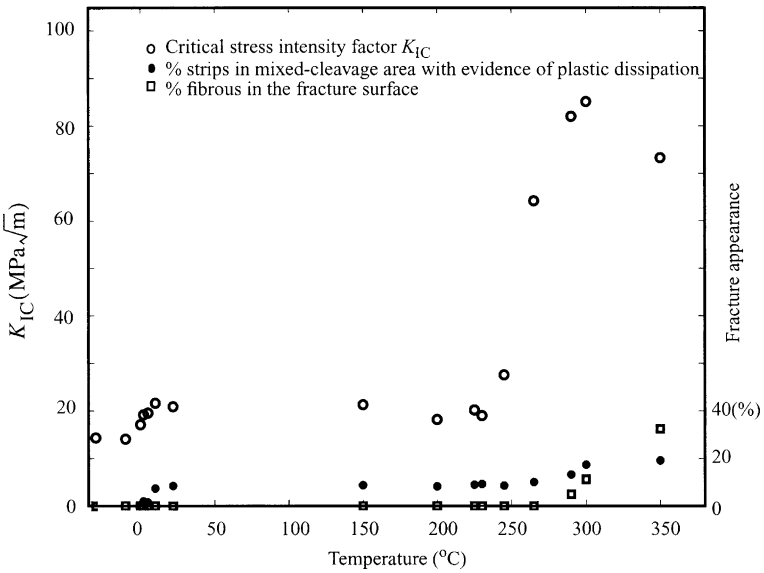

Fig. 3. Temperature dependence of the fracture toughness, K_{IC}, and fracture appearance in coarse grained Fe–2%Si alloy.

the ligaments accounting for the increment in fracture work, over and above, that in the pure cleavage range below the fracture transition. The changing appearance of the fracture surfaces with temperature is shown in Fig. 3 in the form of percent of fibrous fracture.

Fig. 4 shows a SEM micrograph of the fracture surface below the PC/MC transition in the present studies with two grain boundaries that have been traversed. Fig. 5 shows a representative area of the fracture surface above the PC/MC transition, where in addition to the cleavage surfaces of the tiered fracture in grains, noted in the bicrystal study, now appearing as well-delineated river markings, a coarser form of undercutting of adjoining cleavage processes near grain boundaries is visible, associated with plastic bending of a coarser set of ligaments. The appearance of the fracture surfaces remains substantially unchanged from that shown in Fig. 5 between the PC/MC transition temperature and the traditional BD transition around 250 °C. Fig. 6 shows a prominent example of fracture of a remaining coarse ligament between two substantially offset cleavage strips inside a grain in the MC range where the mutual undercutting of the cleavage processes was followed by considerable sigmoidal plastic bending before eventually a complex and jagged cleavage-like fracture process severed the ligament. Another source of quite substantial fracture work, over and above the average fracture work of cracks traversing grain boundaries, is that which is involved when a small fraction of ''recalcitrant'' grain boundaries of large misorientation eventually give way with a very complex ductile shearing and tearing process, after the main fracture front across grains has gone around them and left them behind. An example of the tearing-apart of such a recalcitant grain boundary is shown in Fig. 7.

Fig. 3 shows considerable scatter in the measured K_{IC} results in the plateau region between the two fracture transitions. This is a direct result of

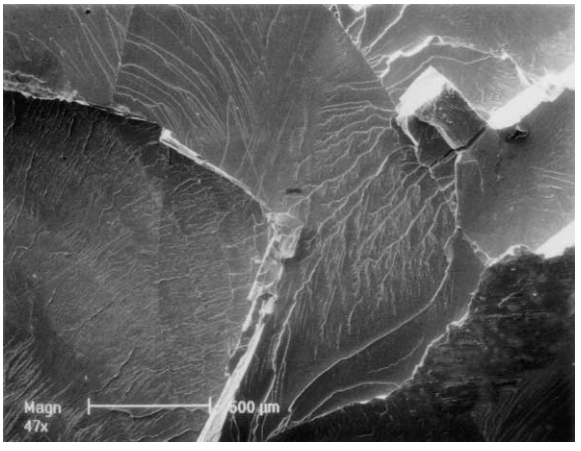

Fig. 4. SEM micrograph of fracture surface of Fe–2%Si below the PC/MC transition at −20 °C. The fracture path is complex, advancing primarily from upper right to lower left, but moving back in the uppermost right region.

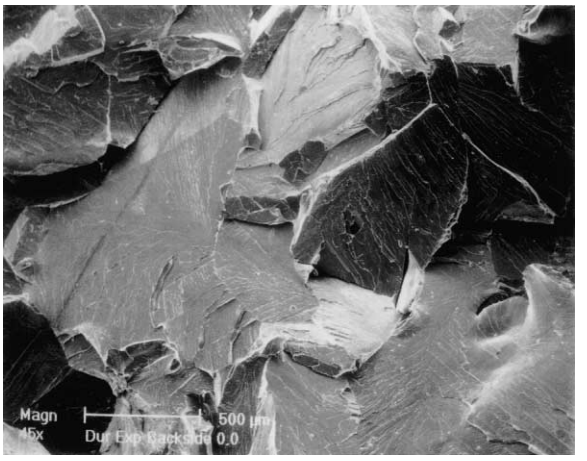

Fig. 5. SEM micrograph of fracture surface of Fe–2%Si above the PC/MC transition at 20 °C.

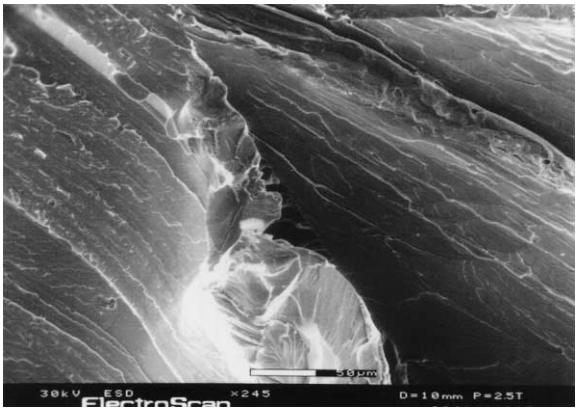

Fig. 6. SEM micrograph of a complex bridging fracture between two parallel cleavage facets inside a grain in Fe–2%Si alloy at −20 °C.

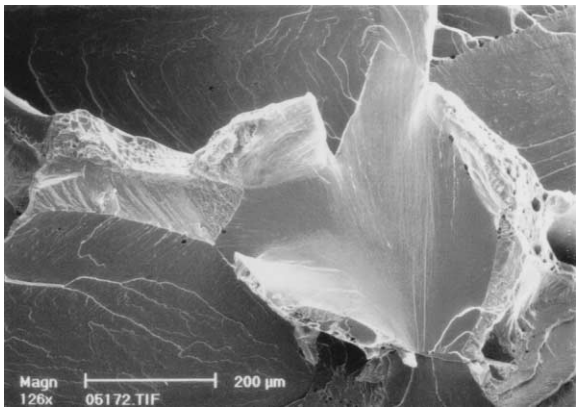

Fig. 7. SEM micrograph of a complex fracture along a recalcitrant grain boundary in Fe–2%Si alloy at −20 °C.

the very coarse grain size in the alloy, making variations between different compact fracture samples large. These variations are less a result of variation of average grain size, but are rather due to the very small number of grains across the critical fracture front where the crack started growing unstably. Thus, between different fracture samples there are large variations in the number of grains across the thickness along the critical fracture front and their respective twist and tilt misorientations between grains along the front. These discrete events and how the main crack percolates through the field of grains is discussed in more detail in Sections 4.2–4.4.

Finally, Fig. 8 shows a region of the fracture surface immediately above the BD transition temperature with a mixture of ductile dimple type separation and continued cleavage type separation. In fact this feature of a strong persistence of terminal cleavage fracture among ductile dimple type fracture remained up to 350 °C, well above the BD transition, and reflected the strong tendency to cleavage of grains in this upper shelf behavior, even after considerable plastic flow in this strongly solid solution strengthened alloy.

3.3. Fracture experiments on the decarburized 1010 steel

The temperature dependence of the fracture toughness of the decarburized 1010 steel is given in

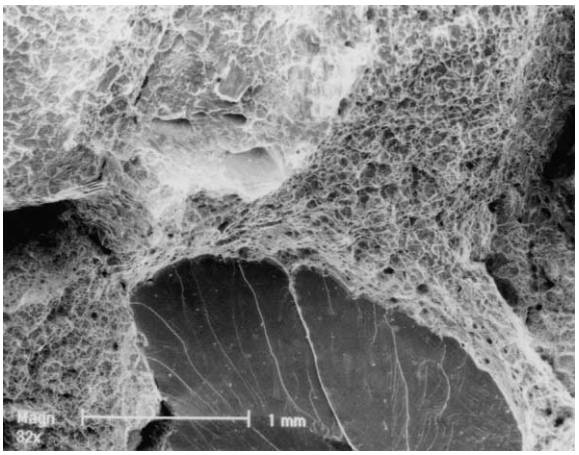

Fig. 8. SEM micrograph of fracture surface immediately above the conventional brittle-to-ductile transition at around 250 °C in Fe–2%Si alloy, showing areas of clear ductile dimple fracture and cleavage fracture.

Fig. 9. Because of the relatively very low plastic resistance of this material the fracture resistance as determined from the DECP samples is given by the *plane stress* J-integral value, J_C, according to well established procedure (Kumar et al., 1981). Clearly, in the temperature range between −150 and 150 °C the material is well above its conventional brittle-to-ductile transition temperature indicated by the level of the measured J_C values. The micrograph of Fig. 10 of the fracture surface at −100 °C shows an area of ductile dimple type separation among cracked grains. Nevertheless, on the whole, as Fig. 9 indicates, the fracture surface appearance is nearly completely of cleavage type and remains so up to −50 °C. This is more clearly demonstrated by the fractographs of Fig. 11(a)–(c) showing representative fracture surfaces at −125, −70, and −40 °C. This upper shelf cleavage response is indicative of the intrinsically brittle nature of Fe where a terminal cleavage mode of separation can still occur after substantial plastic work, and signals a possibility of a troubling tendency to overall terminal brittle behavior in large structures.

The *plane stress* fracture toughness values J_C referred in Fig. 9 in the entire temperature range of −150 to 150 °C are quite large, primarily because of the low plastic resistance of the material devoid

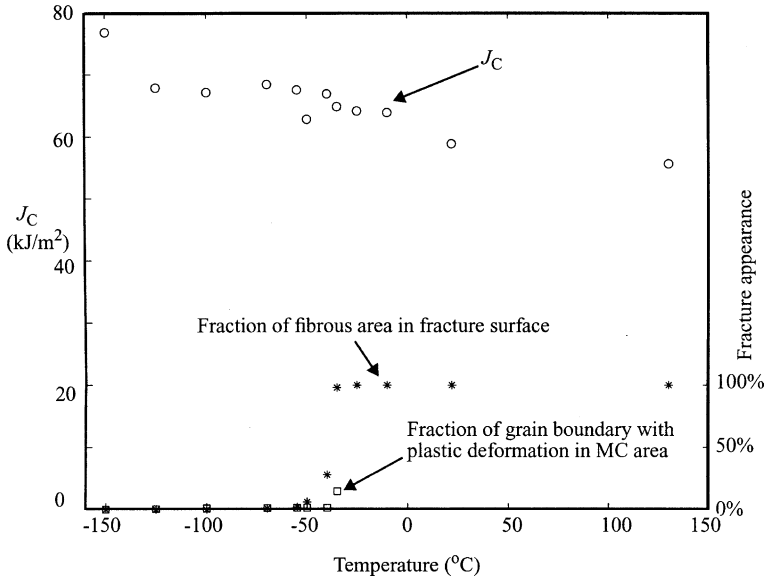

Fig. 9. Temperature dependence of J_{IC} plane stress fracture toughness in DECP specimens of decarburized 1010 steel showing the persistence of terminal cleavage fracture above the brittle-to-ductile transition in the upper shelf region.

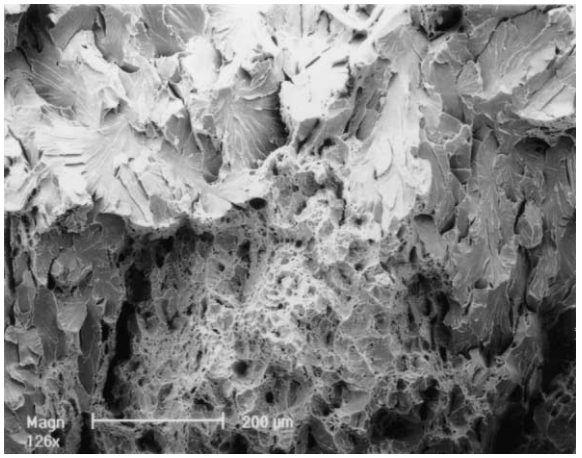

Fig. 10. Fracture surface of decarburized 1010 steel at −100 °C, well above its brittle-to-ductile transition temperature, showing a mixture of cleavage and ductile dimple fracture.

of any significant hardening agent and the elevated brittle strength, estimated to be around 1.0 GPa, based on the moderately small grain size. This has made the DECP sample configuration with the grain dimensions used in this study, more in the nature of a stubby tension specimen, rather than a fracture toughness specimen. Nevertheless, the behavior represented in Fig. 9 is that of a very tough, material in the near-cryogenic temperature range. We discuss this behavior further in Section 5.3 in comparison with the behavior of the Fe–2%Si alloy.

4. Models for percolation of a cleavage front through grains

4.1. Topological features

A subject of primary interest in the present study was the topology of the forms of percolation of a cleavage fracture front through a field of grains and the overall fracture resistance that arises from this process. For this purpose, a number of Fe–2%Si compact fracture mechanics samples were prepared and were fractured in the manner of ASTM standard E339. While the very coarse-grained nature of this material resulted in considerable scatter in the determination of fracture toughness as we indicated in Section 3.2, this was particularly convenient for the detailed study of the percolation of the cleavage front among grains. Such compact fracture experiments were

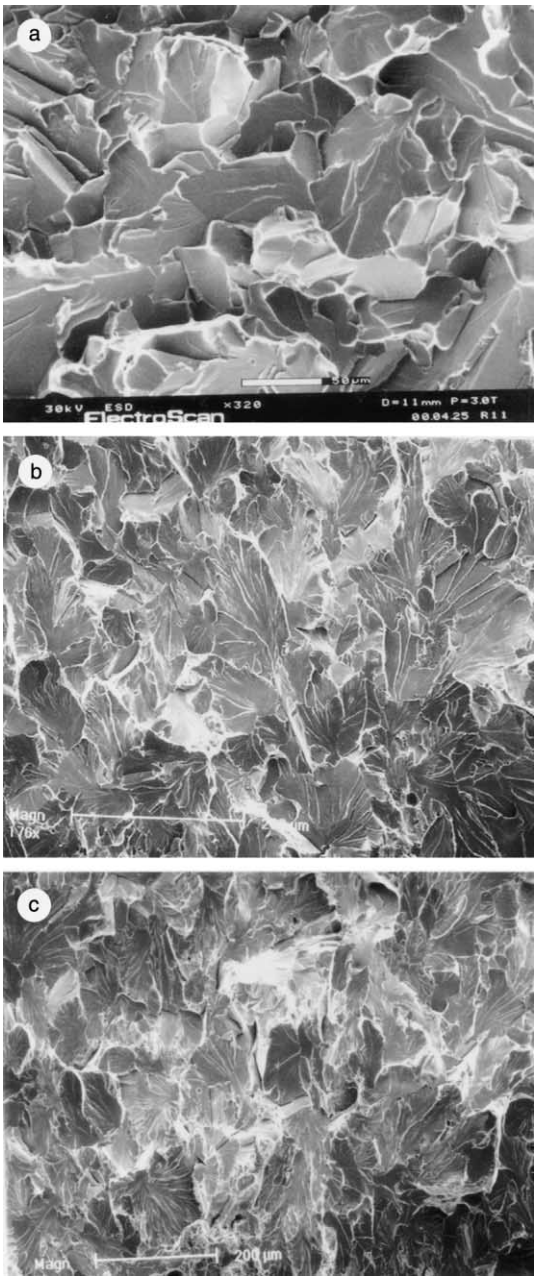

Fig. 11. A sequence of SEM micrographs of fracture surfaces in decarburized 1010 steel: (a) at −125 °C; (b) at −70 °C; and (c) at −40 °C.

performed at −30, 0 and 21 °C. Here we will follow only the features of the percolation of the crack front in the experiment carried out in the pure cleavage realm of −30 °C. During the experiment the crack opening load and the crack opening displacement were recorded. As in other such experiments, it was noted that the crack advanced in a jerky manner, involving, on the average, three jumps before fully unstable separation of the entire specimen occurred. While plastic dissipation at the arrest fronts was slight, for each jerky advance it was relatively easy to identify the fronts of crack arrest through inspection of the field of cleaved grains after the experiment was over, and from the increased compliance of the compact fracture specimen.

Identification of the actual mode of advance of the cleavage front among grains was readily possible, by studying the patterns of cleavage river markings inside grains. While this process could not identify the position of the crack front at given times, it did identify the actual percolation features of the local crack advance from grain to grain. Several detailed features of this advance proved to be interesting and amenable to some detailed modeling as we present in Section 4.3.

On the basis of the earlier bicrystal study (Qiao and Argon, 2003a) where it was established that the primary resistance to crack advance is the resistance of boundaries to the passage of cleavage cracks across them, it was assumed in the present study also that once a cleavage crack penetrated into a grain it would traverse through it nearly instantaneously in comparison to the time spent in overcoming the grain boundaries. In a jerky advance step the crack front traverses across a significant number of grains in very close succession, making inertial effects likely to be important in this process. Nevertheless, in our considerations we ignore these and treat the crack advance as quasistatic. In this idealization, at any stage the further advance of the crack will depend on the local distribution of the momentary crack tip stress intensity K_I. As a further step in the idealization we note that because of the random misorientation of cracked grains immediately behind the crack front the cracked cleavage planes will be misoriented in relation to the average plane of cracking making the "driving forces" at the crack front to be of mixed mode. In our consideration, however, we also ignore this mixed mode nature of advance and

consider only the distribution of the local crack tip mode I stress intensity, K_I, as if the cracked portion of material immediately behind the crack front was flat and in the average plane of the advancing crack. Clearly, these simplifications compromise the accuracy of the model that we present in Section 4.3 with the consequences becoming observable in comparison between model results and actual observations. Finally, the advance of the crack front at any particular grain boundary along the front will depend both on the driving forces and the fracture resistance of the specific boundary. Noting these provisos, a number of important observations are still possible on the topology of the crack advance. These we enumerate below.

We consider a generic square-shaped grain ABCD in the path of the crack front as shown in the cases depicted in Fig. 12, where the shaded region represents the cracked portions immediately behind the crack front. In the case of Fig. 12(a) the crack front encounters and exposes a grain that will be subjected to a significant concentration of local K_I, it then enters the grain from the exposed boundaries AB, BC, and CD simultaneously, or in quick succession. In the case of Fig. 12(b) the crack front encounters a particularly weak grain boundary BC and penetrates through it. While the stress intensity along boundaries BA, AD and DC will be significantly lower because of the re-entrant nature of the initial penetration, the front may still penetrate these boundaries and fan-out from there toward the front and the sides of the grain if the strength of these boundaries are lower than the adjoining boundaries OB and CP along the crack front. When the generic grain occupies a corner position along the crack front as shown in Fig. 12(c) and (d), the corner will again be subjected to a significant excess of the driving force. In this case several possibilities were found to occur. If boundary AB is tougher than the average, the crack will, as depicted by Fig. 12(c), penetrate the grain through the boundary BC first and shear boundary AB later which would then be subjected to a significant mode III driving force. In most cases, however, if the toughness of boundaries AB and BC are close together the crack front can penetrate the grain through these boundaries in quick succession as depicted in Fig. 12(d). Other more complex penetrations were also observed occasionally. Whenever the generic grain is penetrated from more than one side more complex river markings are produced in the grain, making a unique determination of sequences of penetration difficult. While all these modes of cracking of grains were observed, the dominant process was the entry of the main crack into a particular grain across only one boundary as we discuss in Section 4.2.

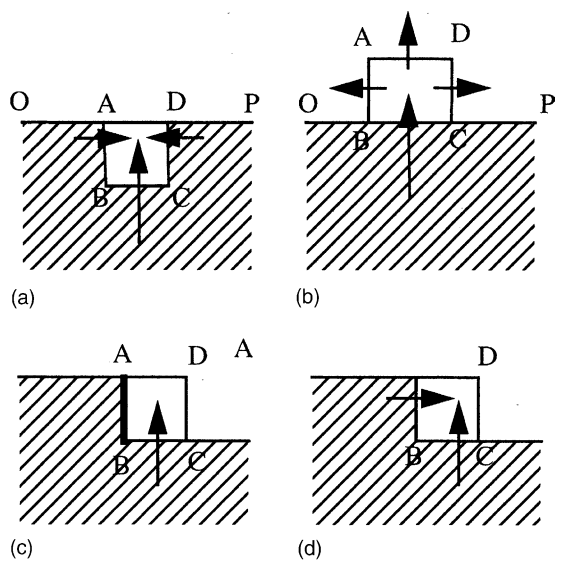

Fig. 12. Various modes of entry of a cleavage front into individual grains: (a) penetration into an exposed grain; (b) penetration into a grain through a particularly weak boundary; (c) and (d) cracks entering into grains with an exposed corner.

In some instances, as already mentioned above, a particular grain boundary may be too tough to be penetrated by the main crack front. Then the front will surround the grain and the "recalcitrant" grain boundary, and leave it behind to be subjected to high levels of combined modes II and III, resulting in eventual overcoming of the boundary by a combination of shear deformation and fracture. Our estimates indicate that the contribution to the overall work of fracture of such tough grain boundaries are significant, and that roughly a fraction of 10–15% of grain boundary line length exposed by the penetrating crack front is of this type.

4.2. A detailed history of percolation of a cleavage front through a field of grains

We now consider in some detail the percolation of a specific cleavage front through a field of very coarse grains in a standard compact sample fractured at −30 °C. Fig. 13 shows a macrograph of the fracture surface in this sample (DC01) of Fe–2%Si alloy. River markings in some grains are discernible in the figure but were very clearly observable in all cases under a magnification of about 50. In this particular sample 78 individual grains were identified between the initial crack tip of the compact fracture sample, along the left border, and a final region close to the other border of the sample. Some grains in the upper and lower right side of the field were not identified as well as some grains at the far right edge. In these regions the crack had been growing already unstably where further details were not of interest. The individual tilt and twist angles of the principal cleavage plane of each grain relative to the external borders of the sample were measured with the special modified stereo microscope illustrated in Fig. 1. These angles, in degrees, are listed in Table 2 for all the 78 grains that were identified. Fig. 14 depicts how the orientational relations of these tilt and twist angles, ψ_0 and φ_0, relative to the normal of the median plane to the crack and the crack growth direction were obtained.

Fig. 13. Macrograph of a fracture surface of a compact fracture specimen of very coarse grained Fe–2%Si alloy. The vertical thickness dimension is 26 mm.

Fig. 15 shows a cleavage front percolation map of the crack penetrations into each grain in this

Table 2
The measured tilt (ψ_0) and twist (φ_0) angles of individual cleavage facets in grains relative to external specimen axes as defined in Fig. 14

Grain number	1	2	3	4	5	6	7	8	9	10	11	12	13	14
φ_0 (°)	−8	−10	11	27	0	−1	−4	8	−15	−4	−6	41	16	17
ψ_0 (°)	12	43	32	−2	−1	−1	−21	−11	−10	−7	−4	9	−22	−32
Grain number	15	16	17	18	19	20	21	22	23	24	25	26	27	28
φ_0 (°)	12	7	10	4	−20	−18	−15	12	−27	−4	8	6	22	25
ψ_0 (°)	18	−41	14	2	−4	−9	28	44	17	−33	−16	−44	−40	−38
Grain number	29	30	31	32	33	34	35	36	37	38	39	40	41	42
φ_0 (°)	−5	−8	−10	−4	13	3	−15	7	16	38	23	32	25	−8
ψ_0 (°)	−5	45	45	36	−15	−18	−24	−20	−2	3	−16	−4	28	−2
Grain number	43	44	45	46	47	48	49	50	51	52	53	54	55	56
φ_0 (°)	−11	6	10	18	−26	−3	−8	5	−11	7	−5	−4	−28	5
ψ_0 (°)	9	3	1	−6	−2	30	11	28	−22	−26	0	0	33	10
Grain number	57	58	59	60	61	62	63	64	65	66	67	68	69	70
φ_0 (°)	3	−37	−21	4	5	27	−11	13	14	11	−7	1	7	−5
ψ_0 (°)	−2	−8	11	15	13	40	−28	−26	−1	−12	−14	5	−15	−4
Grain number	71	72	73	74	75	76	77	78						
φ_0 (°)	5	8	3	3	−1	7	16	7						
ψ_0 (°)	−1	31	6	4	8	−19	−16	−4						

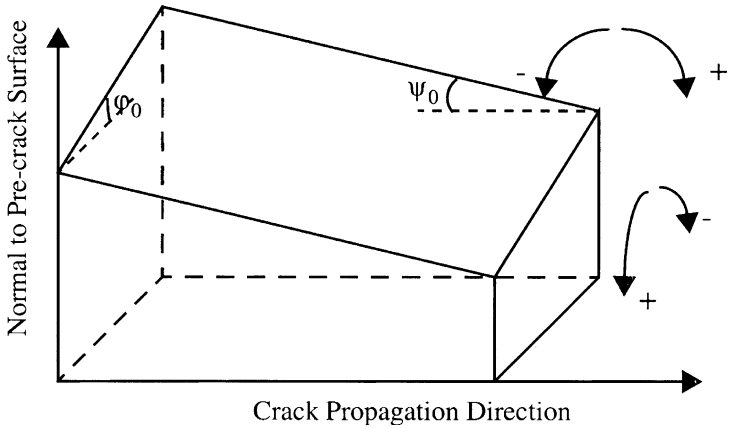

Fig. 14. Orientation relationship of cleavage facets in individual grains, relative to external specimen axes.

sample. The left border of the figure is the initial macro crack tip cut into the compact fracture sample. The solid arrows, based on a detailed study of the river markings fanning-out from grain boundaries, indicate the direction from which the individual grain was penetrated. While this penetration was in many instances from only one direction, there was a number of grains that showed multiplicities of river markings indicating simultaneous, or nearly simultaneous, penetration of the grain from more than one direction. The arrow map shows the spatially complex form of the percolation process. Two specific fronts A–A and B–B have been identified by heavy zigzag lines. These are two fronts of arrest of the jerkily advancing crack, as best as they could be related to the externally monitored crack opening force/displacement information. The final propagation of the crack front beyond the B–B line was in one unstable step. As explained in more detail in the crack front advance model in Section 4.3 it was of interest to glean some insight into the further advance of the crack front from lines A–A and B–B. For this purpose the local mode I crack driving force, K_I, was calculated along the jagged arrested crack front using Rice's (1985) variational method according to the relation

$$K(z) = K_0[z; a(z)] + \frac{1}{2\pi}\int \frac{K_0[z'; a(z)] \cdot [a(z') - a(z)]}{(z' - z)^2}\,\mathrm{d}z' \qquad (1)$$

where $a(z)$ is the crack length at location z along the direction parallel to the sample thickness and roughly parallel to the arrested crack front, $K_0[z; a(z)]$ is the local mode I stress intensity factor at location z in relation to a virtual reference straight crack-front-segment at $a(z)$ under the same remote load. In the evaluation of the integral the principal value was taken, and the upper and lower integration limits were taken as 0 and h, respectively, where h is the specimen thickness. The result of such an evaluation is shown in Fig. 16(a) and (b) for the crack fronts A–A and B–B respectively. The cuspy contours indicate the distribution of the local $K_I(z)$ normalized with the overall stress intensity factor K_0, based on the increased specimen compliance. It is seen that the local crack driving forces for further crack advance are highest at the exposed corners while reentrant corners are protected, as can be expected. The actual local choice for further penetration of the crack front depends also on the fracture resistance of the individual grain boundaries along the front. Nevertheless, there is a satisfactory correspondence between the level of the driving force and the direction of the further crack advance. The dotted stepped contour across each grain boundary represents the actual local normalized energy release rate (or work of fracture) for a virtual extension of the crack across the specific grain boundaries, determinable from the character of the grain boundary.

A number of statistical observations related to the percolation map of Fig. 15 are of interest. Many of the projected grain boundary lines are

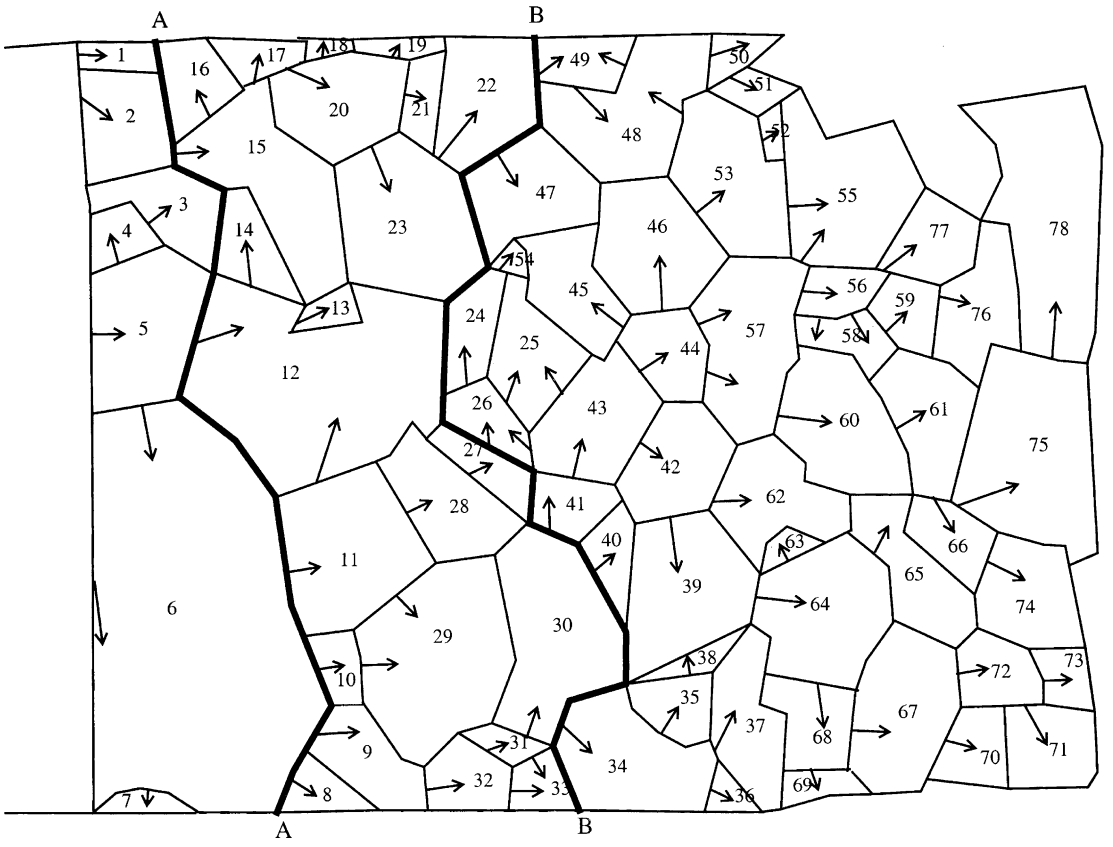

Fig. 15. The cleavage fracture percolation map through the grains of the sample shown in Fig. 13, showing also two crack arrest fronts A–A and B–B.

kinky and some of them have substantial curvature indicating that the grain boundary energy was far from isotropic. Not counting the edges of grains that were free surfaces, the 78 grains possessed 397 edges indicating that the average number of edges of a typical grain was 5.09 rather than 6.0. The frequency distribution of numbers of edges of grains is given in Fig. 17. The arrow map of Fig. 15 indicates that of the 78 grains 67 were penetrated only through one grain boundary while 11 were penetrated from two grain boundaries. This indicates that only 89 grain boundary penetrations governed the form of percolation of the cleavage front across the grains in the particular field. Since each of the 397 boundaries are shared by two grains only a fraction of 0.45 of the boundaries had played a role in the percolation map and the remaining fraction of 0.55 of boundaries separate already cracked grains and must be sheared by a mixture of modes II and III involving a combination of plastic shear and shear fracture. Clearly, of the relatively small number of grains that take part in the percolation process fully 8% of grain edges in the field represented free borders. This makes the statistical information not quite representative of a large fracture surface in a small-grained polycrystalline sample. Nevertheless, this information will be useful in reaching some overall conclusions which we will develop in Section 5.

4.3. Modeling the percolation of cleavage fracture fronts through a field of grains

A special program was developed to model the percolation of a cleavage front in polycrystalline

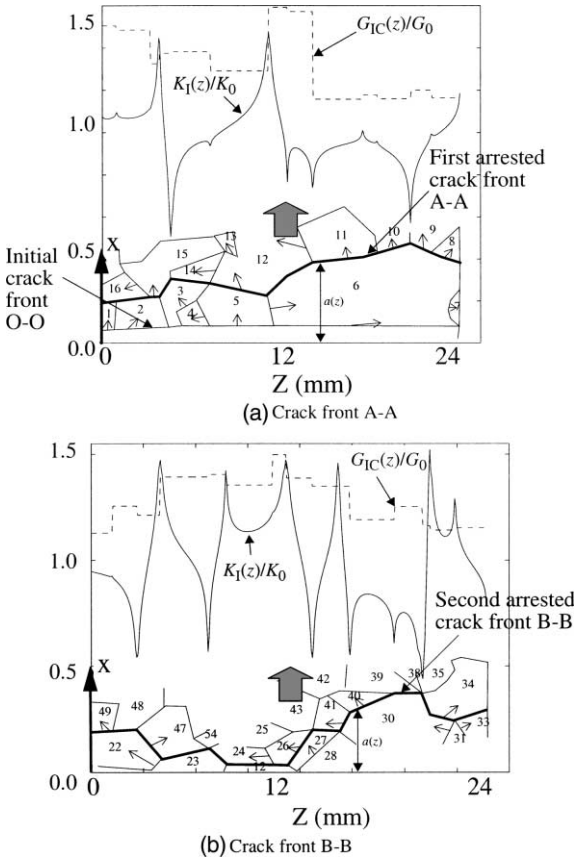

Fig. 16. The calculated distribution of local normalized stress intensity factors $K_I(z)/K_0$ along the fracture fronts A–A and B–B.

material. The principal assumptions of the model were outlined in Section 4.1. The specific grain structure used in the model was that of the compact fracture specimen DC01 of the Fe–2%Si alloy fractured at −30 °C and described in detail in Section 4.2 above. The size and shape of each grain was taken from the macrograph of Fig. 13 and the graphical depiction of it in Fig. 15. The required misorientation angles of the most appropriate cleavage planes of each grain were those listed in Table 2.

The initial straight crack front is given by the left border of the grain field map of Fig. 15. The plane of the pre-crack was considered to be in the median plane of the compact specimen. At the beginning of each propagation step, the effective

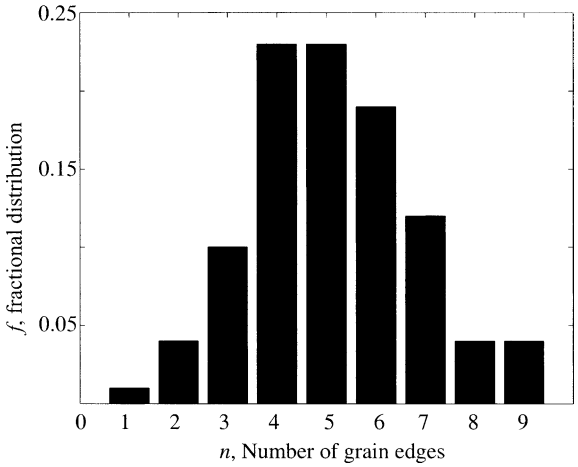

Fig. 17. Histogram showing the distribution of numbers of grain edges in the fracture field of Fig. 15, not counting grain edges bounded by free surfaces.

local crack driving force K_i and the local fracture resistance $G_{IC}^{(i)}$ of each individual grain boundary i ($i = 1, 2, \ldots$) at the crack front were calculated. The effective crack driving force K_i was taken to be the line average of the local stress intensity factor $K(z)$ along the part of the crack front at the grain boundary of interest. The first-order variation method developed by Rice (1985) was used to calculate $K(z)$, according to the expression of Eq. (1) given in Section 4.2. In the numerical integration along the whole crack front, a Romberg algorithm was used (Dahlquist and Bjorck, 1974), which is an application of Richardson's extrapolation to obtain an accurate numerical solution by combining several less accurate solutions of the trapezoidal rule with different step lengths.

The local fracture resistance G_{ICB} of an individual grain boundary used in the model was calculated according to a relationship developed for bicrystal grain boundaries in a previous study for a Fe–3%Si alloy (Qiao and Argon, 2003a) given by

$$\frac{G_{ICGB}}{G_{IC}} = \frac{1}{(\cos\psi)^2}(\sin\varphi + \cos\varphi) + C \cdot \frac{\sin\varphi\cos\varphi}{\cos\psi} \tag{2}$$

where G_{IC} is the average work of cleavage fracture inside individual grains and C is a material constant combining some geometrical features of the

topography of the cleavage surface of a grain interior with the shear resistance of the boundary, leading to an estimated value of $C = 0.25$ according to a best fit to experimental measurements for a wide range of tilt and twist angles of cleavage planes across a grain boundary. The angles ψ and φ are tilt and twist angles of cleavage planes of the adjoining grains across the shared grain boundary and the orientation of the cleavage surface in the grain to be penetrated by the crack front, respectively. These angles are obtained from the external angles φ_0 and ψ_0 reported in Table 2 by expressions

$$\tan\psi = \frac{l_1 \cot\varphi_0 + l_2 \cot\psi_0 + l_3}{n_1 \cot\varphi_0 + n_2 \cot\psi_0 + n_3} \tag{3a}$$

$$\tan\varphi = \frac{m_1 \cot\varphi_0 + m_2 \cot\psi_0 + m_3}{n_1 \cot\varphi_0 + n_2 \cot\psi_0 + n_3} \tag{3b}$$

where

$$l_1 = \cos\psi_1 \cos\alpha - \cos\varphi_1 \sin\psi_1 \sin\alpha \tag{4a}$$

$$l_2 = -\cos\psi_1 \sin\alpha - \cos\varphi_1 \sin\psi_1 \cos\alpha \tag{4b}$$

$$l_3 = \sin\varphi_1 \sin\psi_1 \tag{4c}$$

$$m_1 = \sin\psi_1 \cos\alpha + \cos\varphi_1 \cos\psi_1 \sin\alpha \tag{4d}$$

$$m_2 = -\sin\psi_1 \sin\alpha + \cos\varphi_1 \cos\psi_1 \cos\alpha \tag{4e}$$

$$m_3 = -\sin\varphi_1 \sin\psi_1 \tag{4f}$$

$$n_1 = \sin\varphi_1 \sin\alpha, \quad n_2 = \sin\varphi_1 \cos\alpha, \quad n_3 = \cos\varphi_1 \tag{4g}$$

with α being the angle between the grain boundary line on the fracture plane and the z-axis, and φ_1 and ψ_1 being the twist and tilt angles of the cracked grain immediately behind the crack front. The ratio of $K_i/K_{IC}^{(i)}$ (where $K_{IC}^{i} = \sqrt{EC_{IG}^{(i)}/(1-\nu)^2}$) of each grain boundary along the crack front was considered and the grain boundary with the largest value of the ratio was taken as the one to be penetrated through first by the propagating crack. A factor Q was determined which makes this largest value unity, and was then used to determine the overall applied stress intensity factor K_I on the global sample to advance the crack front through the grain. The propagation of the cleavage crack inside the grain was assumed to be instantaneous, advancing the crack front in the grain of interest. After the grain under consideration was cracked, a new crack front was formed by replacing locally the penetrated grain boundary by the boundaries of the same grain that were not at the initial crack front. Then, the K_i's and $K_{IC}^{(i)}$'s along the new crack front were calculated and the similar procedure was repeated until all the grains in the specimen were cracked. This procedure established the chronology of percolation of the crack front through the collection of grains under the provisos of ignoring inertial effects and possible modes II and III as stated above. Based on this procedure, a fracture map was produced and is indicated by the arrows in Fig. 18 for each grain. When compared with the experimental arrow map of Fig. 15 it is clear that for the first several columns of grains, the model results matched quite well the experimental results. About 70% of the arrows were predicted correctly. However, with continued propagation of the crack, accumulating errors and the increasing complexity of the crack front shape made the model results increasingly less accurate relative to the experimental observations. In the last several columns of grains, only less than 10% of arrows were predicted correctly. This eventual lack of agreement is attributed primarily to the fact that the local crack driving force at grain boundaries is in reality of mixed mode and not merely of the mode I type, and secondarily to the fact that in this terminal sweep of the cleavage front quasi-static conditions will no longer prevail. Since the crack growth becomes unstable beyond the B–B front this eventual lack of agreement is not of importance.

4.4. Model of total work of cleavage through a field of grains

In Section 4.3 we considered only a model of the chronology of the percolation of the cleavage process through the field of grains for comparison with the observed percolation-arrow-map of Fig.

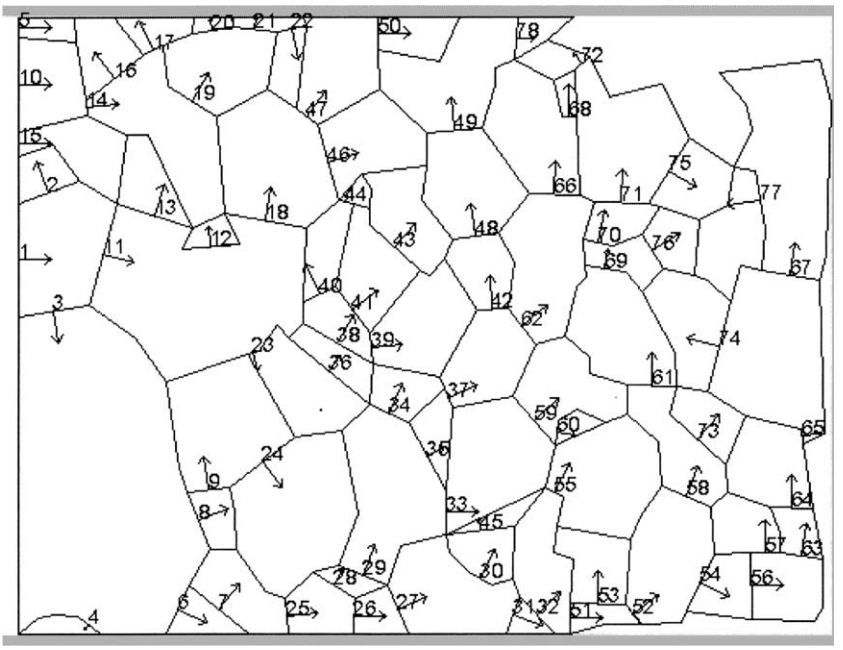

Fig. 18. Computed cleavage fracture percolation map using information on grain boundary resistance determined from Qiao and Argon (2003a).

15. In this section we develop a model to account for the entire work of cleavage fracture in the pure-cleavage (PC) domain at very low temperature where additional plastic dissipation is minimal, but shear fractures along bridging grain boundaries become important. We then project this model to the range of mixed-cleavage (MC) above the pure-cleavage to mixed-cleavage (PC/MC) fracture transition.

We base our model on the basic observations described in Section 4.2 which indicated that in the majority of cases (86% of the time) the cleavage front enters a specific grain from only one neighboring grain. Fig. 19(a) shows a basic set of processes necessary to account for the overall work of cleavage where we idealize outlines of individual grains as square shaped. The arrows show a scheme of spreading of the cleavage front and the boundaries from which the arrows emanate. The spreading requires a special scenario of penetration of a cleavage front across a boundary separating two grains with a combination of tilt and twist misorientation of the cleavage planes across the boundary plane. This specific scenario and the associated resistance of the boundary to the penetration of the cleavage front across it was discussed in detail by us earlier (Qiao and Argon, 2003a).

We identify three separate and distinct contributions to the overall cleavage work per unit area of the projected median macro crack plane, that we view as the extension of the plane of the cleavage crack depicted in Fig. 19(a). The first contribution is the cleavage work across the faces of the grains 1–6 in the figure where each cleavage plane (j) has a specific tilt, ψ_0^j, and twist φ_0^j misorientation angle with respect to the median macro crack plane. These angles are listed in Table 2 for the specific cases of grains shown in Fig. 15, that we will study. The second contribution is the fracture work across the primary boundaries of percolation of the cleavage front, i.e. those from which the arrows emanate in Fig. 19(a). This work of break-through of the primary boundaries was discussed in detail in a previous study referred to earlier (Qiao and Argon, 2003a). The third

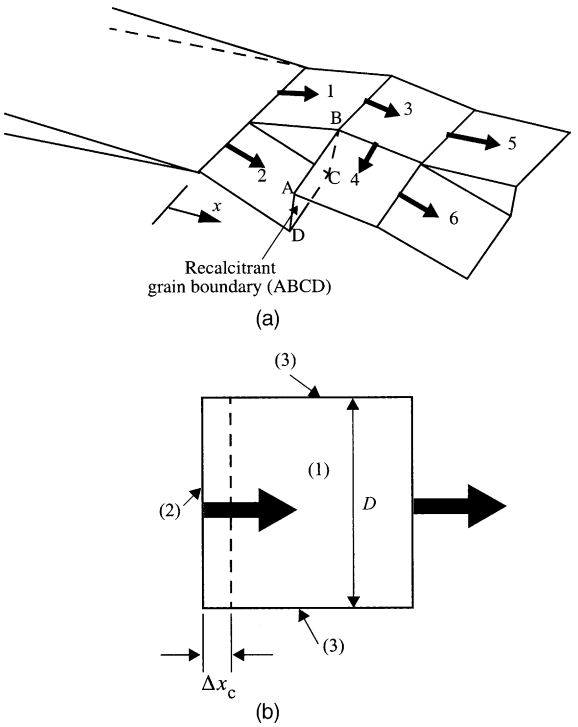

Fig. 19. (a) A schematic view of the types of boundaries overcome by the cleavage front. Boundaries with emanating arrows are those that govern the form of penetration of the fracture front from grain to grain. Boundaries between 1–2, 5–6, and 2–4, in various measure, require extensive fracture work to bridge primary cleavage facets; (b) simplified field in a generic square grain: (1) cleavage work inside grain; (2) work of fracture for going through the principal boundary controlling the percolation process; (3) boundaries requiring large amount of bridging fracture work by plastic shear and cleavage-like separation.

contribution is the subsequent work of separation by a combination of some plastic shear and shear fracture along the boundaries between adjacent grains that have already been cleaved apart, such as the boundaries between grains 1–2, 5–6, and 2–4 depicted in Fig. 19(a). Of these the boundary between 2–4 might be a tougher-than-average recalcitrant boundary that gives way after it is fully surrounded by cleaved grains. For ease of accounting we depict these three contributions for a generic square grain in Fig. 19(b), where the three contributions to the cleavage fracture work are associated with the corresponding numbers.

The fracture work across grain faces is taken as

$$W_1 = \frac{G_{IC}}{\cos\psi_0^j \cos\varphi_0^j}(C_s D^2) \tag{5}$$

where G_{IC} is the specific cleavage work of fracture in a reference grain with cleavage plane exactly parallel to the median macro-cleavage plane, and the angles ψ_0^j of tilt and φ_0^j of twist of the specific grain (j) are given relative to the reference axes of Fig. 14, with $C_s D^2$ being the projected area of the cleavage plane (j) of the grain facet on the median plane. In Eq. (5) D is taken as the length of the grain boundary in the reference square grain, and C_s is a constant determined by grain shape, which is unity for square grains and $2/\sqrt{3}$ for hexagonal grains.

The work of fracture associated with the break-through of a grain boundary is taken as

$$W_2 = G_{IC}\left[\frac{1}{(\cos\psi_i)^2}(\sin\varphi_i + \cos\varphi_i) + C\cdot\frac{\sin\varphi_i\cos\varphi_i}{\cos\psi_i}\right]\cdot D\Delta x_c \tag{6}$$

where the angles ψ_i and φ_i are the tilt and twist misorientation angles of the cleavage planes across the boundary (i) as considered in Eqs. (3a) and (3b), the dimensionless constant C made up of details of shear displacement along the boundary, *cleavage-like* shear fracture resistance of the boundary, microstructural features of the cleavage river markings inside grains and some related coefficients, all defined in the previous study of break-through-resistance of bicrystal boundaries (Qiao and Argon, 2003a). It is taken as $C = 0.25$ on the basis of a single principal fit between experimental measurements and the model of that study, in the range of pure cleavage behavior. The distance Δx_c, as depicted in Fig. 19(b), is the critical average distance of penetration of a reference cleavage front across a grain boundary where the boundary break-through resistance reaches its peak value. This model-sensitive distance is considered to scale with the grain size D for small grain sizes but is expected to be constant for very large grains. It will be assigned a specific magnitude in our model as we discuss below.

Finally, the work of separation of the boundaries left behind by the penetrating cleavage front is taken as

$$W_3 = Dk^*\delta_c\Delta h \tag{7}$$

where δ_c is a critical "preparatory" opening displacement of cleavage planes at the grain boundary plane as depicted in Fig. 20(b) where the boundary separation acquires a "cleavage-like" shear fracture along the average distance Δh between the cleavage planes of the already cleaved adjoining grains, and k^* is the "cleavage-like" shear fracture resistance of the boundary. The boundary length to be shared by the grains is taken as D rather than $2D$, since each lateral grain boundary of a grain to be sheared is shared by two adjoining grains. Clearly, this process of boundary separation involves a mixture of modes II and III of the "cleavage-like" shear fracture and must also depend on the angle of inclination of the boundary with the median macro crack plane. The micrograph of Fig. 21 shows the appearance of such a boundary separated by a combination of shear (the major portion with clearly shown shear markings) and a complex fracture process (identified with the arrow). McClintock (1997) has developed a more detailed model of this bridging shear fracture based on earlier slip line field analysis (McClintock and Clerico, 1980) which results in very similar observations but using a considerably different scenario of separation involving only plastic "shearing off". None of these details which can be expected to be quite model-sensitive and variable from boundary to boundary will be developed further. Rather, as had been done in the previous study of cracking across bicrystal boundaries, referred to above, we introduce a dimensionless parameter B that normalizes this work of separation with the principal specific cleavage work G_{IC} as

$$B = \frac{K^*\delta_c\xi}{G_{IC}} \tag{8}$$

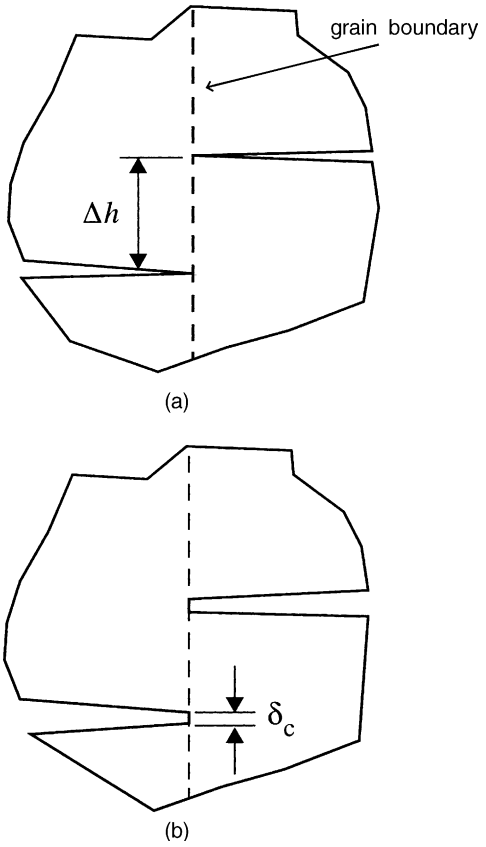

Fig. 20. Stages of bridging fracture work: (a) initial outline of grain boundary bridging primary cleavage facets; (b) preparatory plastic crack tip displacement triggering subsequent "cleavage-like" separation.

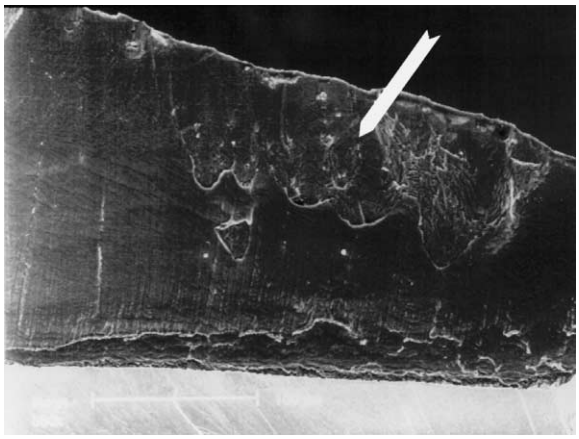

Fig. 21. SEM micrograph of the surface of separation by shear in a typical boundary connecting two cleaved facets in adjacent grains. Most of the surface shows signs of plastic shearing. Portion identified by an arrow shows a fracture type separation.

where

$$\xi = \frac{\Delta h}{D} \tag{9}$$

is the ratio of the average vertical separation Δh between the cleavage planes of the adjacent grains to the mean (square-shaped) grain size. This latter ratio can be expected to depend on the angles of misorientation between the cleavage planes of the adjoining grains. Moreover, as depicted more realistically in Fig. 19(a), the distance Δh locally should depend on the distance x of penetration of the cleavage front across the two adjoining grains and the separation should have a mixed mode character of II and III of fracture as noted above, since none of this detail is realistically amenable to analysis for every boundary, as must be clear, the choice of a single average fitting parameter B becomes very attractive. Thus, combining these three contributions into a single specific cleavage work, G_{ICPC} of the *polycrystal* median fracture plane, in units of the basic work of cleavage, G_{IC}, of a reference grain of no misorientation gives

$$\frac{G_{\mathrm{ICPC}}}{G_{\mathrm{IC}}} = \frac{C_{\mathrm{S}}}{\langle \cos\psi_0^j \cos\varphi_0^j \rangle} + \left(\frac{\Delta x_{\mathrm{c}}}{D}\right) \left\langle \left[\frac{1}{(\cos\psi_i)^2} (\sin\varphi_i + \cos\varphi_i) + C \cdot \frac{\sin\varphi_i \cos\varphi_i}{\cos\psi_i} \right] \right\rangle + B \tag{10}$$

where the brackets across the first and second terms on the RHS of Eq. (10) indicate an orientation average of all possible cases of sampling of grains of random orientation. Rather than develop this expression as given, we consider a model of the above ratio for each grain in the specific case of the polycrystal field considered in Fig. 15 and obtain the cumulative work of fracture for the quasi-statically advancing cleavage front according to the modeled percolation map of Fig. 18. The result of this model, following along the same set of steps developed in Section 4.3 for the determination of the percolation arrow map of Fig. 18, is shown in Fig. 22. In the model, the critical penetration depth Δx_{c} for break-through of a grain boundary was taken as 10 μm for the very coarse-grained material modeled here. Since in the present

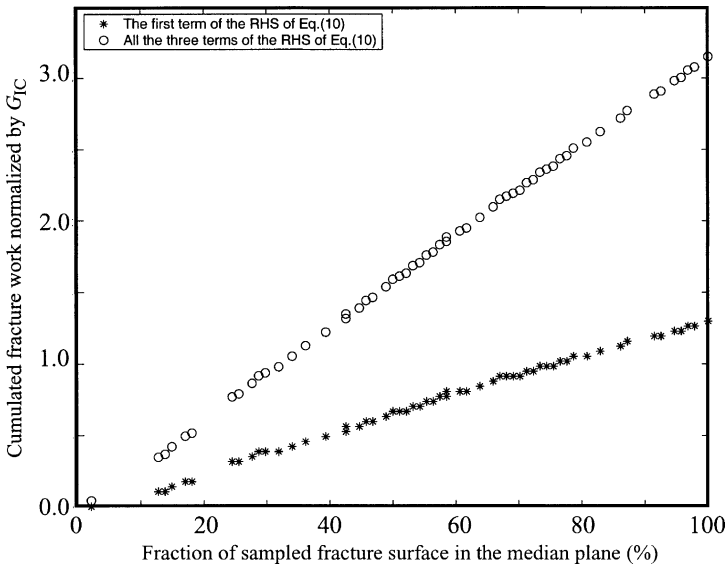

Fig. 22. Result of computer simulation of overall fracture work for an advancing crack front through the family of grains shown in Fig. 15. Stars indicate accumulated fracture work due to cleavage of grain interiors, open circles indicate cumulative fracture work contributed by the severence of the bridging grain boundaries.

case the average grain sizes were in the range of 4mm the ratio $\Delta x_c/D$ becomes roughly 0.0025, making the contribution of the second term in Eq. (10) negligible for such large grain size material. As stated above, for very fine grain material, we assume that Δx_c should become proportional to the grain size, where the second term in the RHS of Eq. (10) will make a non-negligible contribution. In the present context if B is chosen as 1.86, the model results would produce a perfect fit to the experimental results. Thus, the experimentally measured $K_{ICPC} \cong 13$ MPa$\sqrt{m}$ of the polycrystal at −30 °C as indicated in Fig. 3, while $K_{ICSC} \cong 7.3$ MPa$\sqrt{m}$, as measured in connection with crack arrest experiments in Fe–3%Si alloy (Qiao and Argon, 2003b), gives

$$G_{ICPC}/G_{ICSC} = (K_{ICPC}/K_{ICSC})^2 = 3.17 \tag{11}$$

On the other hand the model results indicate that $(W_1/G_{IC}) = 1.31$, in Eq. (10), and since the contribution of the second term is negligible in the present context, to obtain $(G_{ICPC}/G_{ICSC}) = 3.17$, $W_3/G_{IC} = B$ must be chosen as 1.86. In this connection it is worth noting that the contribution of the cleavage work of the grain interiors is 31% higher than G_{ICSC}, the work of planar fracture, due to the random misorientation of the principal cleavage planes in grains, along the entire fracture surface.

Parenthetically, we note that the choice of the magnitude of the constant B as 1.86, and taking $\delta_c \approx \Delta x_c = 10$ μm, $\Delta h/D \approx 0.5$ and $G_{IC}(= G_{ICSC}) = 230$ J/m^2, derived from the average fracture toughness of 7.3 MPa$\sqrt{m}$, measured in a thermal crack-arrest experiment in single crystals of Fe–3%Si alloy (Qiao and Argon, 2003b), would give for the "cleavage-like" shear resistance k^* a value of about 86 MPa. This value of k^* is considerably lower than the plastic shear resistance of the alloy at −30C which is estimated to be in the range of 200 MPa. This indicates that under the present considerations the shear fracture process along the bridging grain boundaries could have only a minor plastic shear contribution, unlike in the model considered by McClintock and Clerico (1980). However, since there is considerable flexibility in the above estimates and Fig. 21 shows clear evidence of plastic shear along bridging grain boundaries, a firm conclusion is not possible on which mode of shear is most likely.

5. Discussion

5.1. Contribution of grain boundaries to the cleavage resistance

Based on the detailed considerations of the percolation of cleavage fracture across a field of grains in the coarse-grained Fe–2%Si alloy discussed in Section 4.2 and the models of the percolation map and work of fracture developed in Sections 4.3 and 4.4, it becomes possible to state a general expression for the contribution of grain boundaries to the overall work of fracture of a polycrystal in the extreme lower shelf region of fracture, labeled by us as pure cleavage (PC) fracture regime. The expression we propose is a generalization of Eq. (10), benefiting from the numerical model of Section 4.4. For this purpose we re-state Eq. (10) in its final form below as

$$\frac{G_{ICPC}}{G_{IC}} = \left\langle \frac{C_s}{\cos\psi_0^j \cos\varphi_0^j} \right\rangle + \alpha\beta\left(\frac{\Delta x_c}{D}\right)\left\langle \frac{1}{(\cos\psi_i)^2}(\sin\varphi_i + \cos\varphi_i) + C\cdot\frac{\sin\varphi_i\cos\varphi_i}{\cos\psi_i}\right\rangle + B \tag{12}$$

In Eq. (12) in the first term on the RHS $C_s = 2/\sqrt{3}$ is a factor correcting for hexagonal-shaped grain facets over the square-shaped grain facets considered in the preliminary rough model; the orientation average of the projection product in brackets is readily evaluated as 1.26 using the data of Table 2. In the second term $\alpha = \sqrt{3}$ is the ratio of the average grain diameter to the grain edge length of a hexagonal grain and the factor $\beta = 1.14$ accounts for the fact that in 14% of cases in the simulation a cleavage crack enters a grain through two faces nearly simultaneously; the orientation average of the term in brackets can be taken as 1.61, as the average value of this factor determined in a previous study of cleavage cracking resistance of bicrystal boundaries (Qiao and Argon, 2003a).

The ratio $\Delta x_c/D$ in this term remains somewhat elusive since the effective penetration distance Δx_c across a boundary where the peak resistance is encountered can only be conjectured. We have arbitrarily considered this dimension to be around 10 μm for very large grains with $D \gg \Delta x_c$. As stated above, however, we consider the ratio $\Delta x_c/D$ to remain a constant for $D \leqslant 10$ μm. In any event we note that the second term is the only one with a grain size dependence, which becomes negligible for very large grain sizes and becomes grain size independent for medium to small grain size material. Finally, as discussed in Section 4.4 above, we have chosen the magnitude of B as 1.86 based on the model of the rate of increase of cleavage fracture work across a field of coarse grains as given in Fig. 22. This gives the final form of the cleavage resistance of the polycrystals as

$$\frac{G_{ICPC}}{G_{IC}} = 1.45 + 3.03(\Delta x_c/D) + 1.86 \quad (13a)$$

$$= 3.31 + 3.03(\Delta x_c/D) \quad (13b)$$

where G_{IC} is equal to G_{ICSC} of single crystals. [2]

We have written Eq. (13a) deliberately in an expanded form to indicate that the contribution to the overall cleavage work of the cleavage of individual grain interiors is substantial and represents roughly 44% of the total work of fracture, as should be clear from Fig. 22. The second term on the RHS of Eqs. (12) and (13a) makes a negligible contribution to the total work of fracture for the large grain material that we have considered specifically even though it is this term that governs the selection of the sites for cleavage break-through across grain boundaries. However, because of the tiered nature of the cleavage break-through across grain boundaries described in the earlier bicrystal study (Qiao and Argon, 2003a) where the majority of break-throughs had been noted to follow a regular mode of penetration, only a relatively small overall change of fracture area results as the cleavage front crosses a typical grain boundary. The somewhat more substantial contribution (roughly 56%) to the overall work of fracture results from the process of *cleavage-like* shear separation along grain boundaries (Fig. 20) between primary cleavage cracking facets in adjoining grains, as had already been concluded by McClintock (1997).

Finally, we return to the exploration of a grain size dependence of the cleavage fracture work. While no important grain size dependence is evident in our model beyond the weak and unimportant grain size dependence represented in the second term of the RHS of Eqs. (12), (13a) and (13b), we have examined the specific effect experimentally. This dependence was probed through fracture toughness determinations at −20C in the pure cleavage range in eight coarse-grained samples, in which the average grain size varied between 1.5 and 6.0 mm. The result is given in Fig. 23. It shows very substantial scatter among the measurements, with no discernable grain size dependence in this narrow range of grain sizes, which is consistent with our model in which the only grain size dependent contribution might conceivably arise for grain sizes in the range of 50–100 μm but should be negligible in the coarse grain size range of 1–10 mm, and disappear for very small grain size material if the ratio $\Delta x_c/D$ reaches a

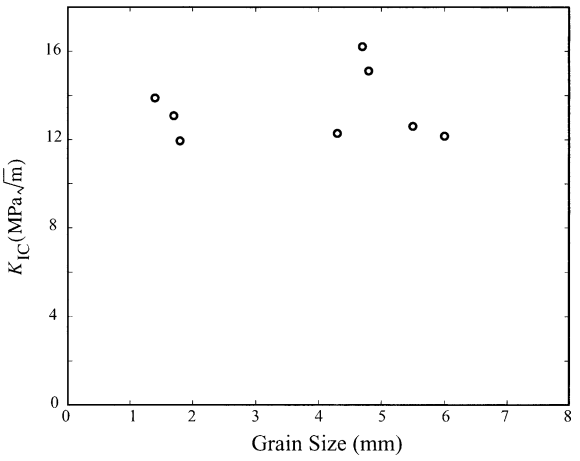

Fig. 23. Grain size dependence of critical stress intensity of fracture at −20 °C in Fe–2%Si alloy.

[2] Our analysis above gives $W_1/G_{IC} = 1.45$, while the simulation model gave this ratio as 1.31 as shown in Fig. 22. We attribute the discrepancy to the factor C_s which apparently is smaller than $2/\sqrt{3}$, in keeping with the observation in Section 4.2 which gave the average grains to be closer to 5 sided.

constant value asymptotically, as was assumed might be the case.

We note that in our model a certain grain size dependence is still possible on a different interpretation of W_3 in Eq. (7), of the work of separation of the boundaries left behind by the primary cleavage penetrations. In that model the parameter δ_c represented a critical shear displacement along the step height of Δh connecting the cleavage planes. This distance was taken to be a constant, independent of grain size, on the interpretation of it being a preparatory step which initiates an abrupt "cleavage-like" separation, terminating all contact between adjacent faces. If on the other hand the separation were entirely by a plastic shearing-off process along the step height Δh, the parameter δ_c should have been $\Delta h/2$ and grain size dependent. This would make the factor $B = k^*\xi^2 D/2G_{IC}$ defined in Eq. (8), and would introduce a direct grain size dependence into the last term of Eq. (10). Such a dependence would be inkeeping with the well known direct dependence of the work of separation of ductile fracture, and still have the correct dependence for asymptotic behavior of a monotone decrease in grain size. However, we have insufficient evidence for such pure plastic behavior and prefer the "cleavage-like" separation mode.

5.2. General observations

The role of grain boundaries and grain size effects in the plastic resistance of polycrystalline metals, particularly steel, has been well appreciated for many decades and has been modeled by Hall (1951) and Petch (1953) among others. Similarly, the effect of grain size on fracture and the beneficial consequence of grain refinement in increasing the brittle strength of steels is well known (Petch, 1954). Furthermore, the triggering effects of fracturing grain boundary carbides in initiating brittle behavior in fracture transitions have also been studied to some extent (McMahon and Cohen, 1965; Ritchie et al., 1973; Lin et al., 1986; Petch, 1986), as we had already noted in Section 1. Outside of these general considerations of grain size effects and phenomena related to triggering of brittle behavior in fracture transitions, specific considerations of the influence of grain boundaries on the cleavage cracking resistance have been few. Of these studies the most noteworthy have been those of Gell and Smith (1967), Anderson et al. (1994) and McClintock (1997). In the work of Anderson et al. (1994), the mode of cleavage fracture across hexagonal grains was considered in some detail to develop realistic cumulative probability distributions of fracture resistance in the context of "weakest link" models of such behavior. Gell and Smith (1967) have made one of the earliest observations on the cracking resistance of individual grain boundaries with known tilt and twist components, in hydrogen charged polycrystalline Fe–3%Si alloy and demonstrated that the major contribution to the cracking resistance of a grain boundary comes from its twist misorientation across the boundary rather than the tilt misorientation. This basic observation, also conjectured by McClintock (1997), was demonstrated directly by us in our earlier bicrystal study (Qiao and Argon, 2003a). The most detailed study of the cleavage cracking resistance of polycrystals, with which we will compare our findings is that of McClintock (1997), who has modeled the form of percolation of a cleavage cracking front across an array of randomly misoriented cubic grains. In his study McClintock makes a series of assumptions that have actually been observed, in part, in the present experimental study. These included the following: that (a) grains crack by a cleavage crack entering them from a neighboring grain rather than when the local resolved normal stress across the best available cleavage plane reaches a critical value, (b) a tilt misorientation across a boundary is far less of an obstacle for penetration of a boundary than a twist misorientation, (c) normal expectations apply that cracking in re-entrant channels formed by cleaved adjacent grains do not readily extend while exposed corners on crack fronts are favored for cleavage propagation, and (d) certain difficult-to-shear boundaries connecting facets of already cleaved grains (recalcitrant grain boundaries) effectively hold back the propagating cleavage front. While some conclusions of the McClintock model such as an excessive tendency of cracking fronts to advance parallel to the front

by laterally propagating cleavage "kinks" along the front, was not found in our observations, many other features were quite similar. The single major departure, however, between the predictions of McClintock and our model has been that the fracture toughness in his model exhibits a square-root type of grain size dependence (linear grain size dependence of work of fracture) while no such grain size dependence resulted from our model. This difference results primarily from McClintock's consideration that the cleavage work of fracture of grain interiors is negligible in comparison with the plastic bridging shear work along boundaries connecting primary cleavage facets, and that the latter process is indeed a plastic shearing-off process. In our model the cleavage work of grain interiors makes up fully one third of the overall fracture work and the bridging shear processes are viewed more as a *cleavage-like* shear fracture in which the traction drops abruptly to zero after a preparatory constant shear displacement emanating from the cleavage facets as depicted partly in Fig. 20 rather than a continuous linear drop characteristic of a pure plastic shearing-off process. Nevertheless, since there are significant uncertainties in both our model and that of McClintock the exact nature of grain size dependence of the cleavage resistance remains unanswered. In any event it is clear that in the very large grain size limit there is no observable dependence which is in support of our model.

5.3. The decarburized 1010 steel

The experimental excursion into the behavior of the 1010 steel was made for the purpose of demonstrating that the findings on the Fe–2%Si alloy could be used in applications to low carbon steels. We note that our findings on the role of grain boundaries on the cleavage fracture resistance of the Fe–2%Si alloy are primarily of a geometrical nature exhibited by the strongly solid solution strengthened single phase bcc material. Thus, the potential applicability of these findings to low carbon steel is appealing. In our experiments with the decarburized 1010 steel where a potentially complicating pearlite component was removed a full demonstration of a parallel behavior to the Fe–2%Si alloy was not quite possible because of the much reduced level of plastic resistance of the former shown in Fig. 2 that resulted in all fracture measurements on the 1010 steel to be effectively on the upper shelf, even at the lowest test temperature of −150 °C. This was evident from the large distortions of the DECP specimens at fracture and relegates the fracture work measurements of J_C to being of plane stress type. Nevertheless, much can be concluded from the cleavage fracture surface features shown in Fig. 11(a)–(c), albeit all being in the nature of terminal cleavage occurring after very substantial amounts of expanded plastic work in the ligament between the two edge cracks. The fracture surface of Fig. 11(a) at −125 °C shows a field of cleaved grain facets of a distinctly brittle appearance with only weakly delineated river markings which we would have expected to be quite similar to those observable in the pure cleavage realm at the lower shelf below the ductile-to-brittle (DB) transition temperature. However, in the present case, because of the reduced level of the plastic resistance of the material due to decarburization and on the basis of our estimation of the brittle strength of the 1010 steel, we expect that the BD transition will be in the liquid nitrogen temperature range. Nevertheless, the fracture appearance in Fig. 11(b) at −70 °C, now well above the DB transition, still shows a field of cleaved grains, but with well-delineated cleavage river markings, giving clear evidence of accompanying plastic distortions resulting from the bridging deformations between grains.

The most profound observation derivable from the comparison of the behavior of the Fe–2%Si alloy and the decarburized 1010 steel is the dramatic reduction in the conventional ductile to brittle transition temperature by about 400 °C, from 250 °C (for the Fe–2%Si) to −150 °C (for the decarburized 1010 steel) when all hardening agents are removed from the Fe. We note that this effect is far larger than what might be expected from inspection of Fig. 2 and the shift of the temperature dependent plastic resistance curves. This further accentuation of the difference between the DB transitions results from the fact that the J_C measurements for the 1010 steel are of a plane stress

type in the DECP specimen of quite inadequate size and shape while the results for the Fe–2%Si alloy were derived from bona-fide plane strain test configurations.

6. Conclusions

In the lower shelf in Fe–2%Si and in low carbon steels cleavage cracks percolate through grains by selectively going through the most exposed grain boundaries with the lowest penetration resistance and subjected to the largest local crack driving forces. While these grain boundaries govern the overall chronology of cleavage crack percolation they contribute little to the overall fracture resistance.

The overall fracture resistance is derived roughly in one part by the cleavage resistance of individual misoriented cleavage facets in grains and in two parts by the work of fracture along nearly vertical boundaries bridging the primary cleavage facets of adjoining grains by a combination of plastic shear and a "cleavage-like" shear separation.

Both experiments and modeling of crack percolation mechanisms suggest that the overall cleavage fracture resistance due to the tesselation of the cleavage fracture process by the grain boundaries is largely grain size independent, but increases the fracture resistance (G_{ICPC}) in comparison with a flat untesselated cleavage process (G_{ICSC}) by a factor of close to 3.0.

Experiments carried out on decarburized 1010 steel indicate that, when present, the percolation of cleavage across grains in the upper shelf region is very similar to that in the lower shelf, which has important implications in the triggering of brittle behavior in structures undergoing initial ductile forms of fracture.

Acknowledgements

This research has been supported by the National Science Foundation under grant DMR-9906613. We are also grateful to Professor L. Anand for providing the coarse grained Fe–2%Si alloy plates and to Professors F.A. McClintock and D.M. Parks for useful discussions.

References

Anderson, T.L., Stienstra, D., Dodds, R.H., 1994. A thermodynamical framework for addressing fracture in the ductile–brittle transition region. In: Landes, J.D. et al. (Eds.), Fracture Mechanics: Twenty-fourth Volume, ASTM-STP 1207, ASTM, Philadelphia, p. 186.

Argon, A.S., Qiao, Y., 2002. Cleavage cracking resistance of high angle grain boundaries in Fe–3%Si alloy, Phil. Mag., in press.

Birks, N., 1969. Decarburization, The Iron and Steel Inst., London.

Brown, S.B., Kim, K.H., Anand, K., 1989. An internal variable constitutive model for hot working of metals. Internat. J. Plasticity 5, 95.

Crocker, A., Smith, G., Flewitt, P., Mo skovic, R., 1996. In: Proceedings of the 11th European Conference on Fracture (ECF11), Eng. Mater. Advis. Serv., Warley, UK, Vol. 1, p. 233.

Dahlquist, G., Bjorck, A., 1974. Numerical Methods. Prentice-Hall, Englewood Cliffs, NJ.

Gell, M., Smith, E., 1967. The propagation of cracks through grain boundaries in polycrystalline 3%silicon–iron. Acta Metall. 15, 253.

Hall, E.O., 1951. The deformation and ageing of mild steel: III—Discussion of results. Proc. Phys. Soc. B 64, 747.

Kumar, V., German, M.D., Shih, C.F., 1981. An engineering approach for elastic–plastic fracture analysis, EPRI Report NP-1931, Electric Power Research Institute, Palo Alto, CA.

Lin, T., Evans, A.G., Ritchie, R.O., 1986. A statistical model of brittle fracture by transgranular cleavage. J. Mech. Phys. Solids 34, 477.

McMahon, C.J., Cohen, M., 1965. Initiation of cleavage in polycrystalline iron. ActaMetall. 13, 591.

McClintock, F.A., 1997. A three-dimensional model for polycrystalline cleavage and problems in cleavage after extended plastic flow or cracking. In: Chan, K.S., (Ed.), George Irwin Symposium on Cleavage Fracture. TMS, Warrendale, PA, p. 81.

McClintock, F.A., Clerico, M., 1980. The transverse shearing of singly-grooved specimens. J. Mech. Phys. Solids 28, 1.

Petch, N.J., 1953. The cleavage strength of polycrystals. J. Iron Steel Inst. 174, 25.

Petch, N.J., 1954. The fracture of metals. In: Chalmers, B., King, R. (Eds.), Progress in Metal Physics. Pergamon Press, London, vol. 5, p. 1.

Petch, N.J., 1986. The influence of grain boundary carbide and grain size on the cleavage strength and impact

transition temperature of steel. Ada Metall. 34, 1387.

Qiao, Y., Argon, A.S., 2003a. Cleavage cracking resistance of high angle grain boundaries in Fe–3%Si alloy. Mech. Mater., in press. PII: S0167-6636(02)00284-3.

Qiao, Y., Argon, A.S., 2003b. Brittle to ductile transition of cleavage fracture by thermal crack arrest in Fe–3%Si single crystals, in press. PII: S0167-6636(02)00293-4.

Rice, J.R., 1985. First-order variation in elastic fields due to variation in location of a planar crack front. J. Appl. Mech. 52, 571.

Ritchie, R.O., Knott, J.F., Rice, J.R., 1973. On the relationship between critical tensile stress and particle toughness in mild steel. J. Mech. Phys. Solids 21, 395.

Thelning, K.-E., 1984. Steel and its Heat Treatment. Butterworth, London.